

# Two-way Antagonistic Shape Actuation Based on the One-way Shape Memory Effect

A. Y. N. SOFLA,\* D. M. ELZEY AND H. N. G. WADLEY

*Department of Materials Science and Engineering, University of Virginia  
Charlottesville, VA 22904, USA*

**ABSTRACT:** The stress created by the austenite transformation of mechanically constrained NiTi shape memory alloys (SMAs) significantly exceeds that required to deform (detwin) its low temperature martensitic phase. The one-way shape memory effect can therefore be used to create antagonistic, fully reversible flexural shape morphing structures by assembling opposing pairs of linear contractile SMA actuators. These structures possess two distinct inactive configurations, neither of which requires continuous power for shape retention making them potentially suitable for long-term applications. Here, the shape changes of a representative antagonistic flexural unit cell have been experimentally evaluated, and the effect of the pre-strain of near equiatomic NiTi alloys on the actuation strain has been analyzed and discussed. The predicted deformations are then successfully compared to the response of prototype actuators.

*Key Words:* shape memory, smart structure, antagonistic, morphing, actuator, robotics.

## INTRODUCTION

NUMEROUS groups have sought to design shape-changing structures using active materials such as shape memory alloys (SMAs) (Otsuka and Wayman, 1998) and piezoelectric ceramics (PZT) (Uchino, 1997) that undergo dimensional changes upon application of a suitable stimulus (Wada, 1990; Crawly, 1994; Takagi, 1999; Giurgiutu, 2000; Grag et al., 2001). Other active materials, such as electrostrictive polymers (Perline et al., 1992) and shape memory polymers (Tobushi et al., 1992) have not yet been successfully implemented in the design of load bearing actuated structures due to their small actuating stress. SMAs, however, are attractive as an actuating material because they produce large actuation stresses (hundreds of MPa) and possess a relatively high recoverable shape memory strain (several percent) (e.g., Otsuka and Wayman, 1998).

Pre-stretched, one-way SMA linear actuators contract upon heating above a critical (austenite start) temperature (Otsuka and Wayman, 1998). However, in the absence of an applied tensile load these one-way SMA actuators do not 're-stretch' upon cooling. Actuated structures using one-way SMA actuators are therefore used in conjunction with a bias force-creating component (e.g., a spring, elastic member, or dead weight) (Duerig et al., 1990). Many reversible, SMA-actuated

structures based on this principle have been designed and tested. One approach has embedded one-way SMA wires or ribbons in polymers whose elastic deflection provides the restoring force (Pfaeffle et al., 1993; White and Berman, 1998; Baz et al., 2000). A second approach has one-way SMA elements directly attached to shape changing structures containing elastic members (e.g., springs) for shape restoration (Beauchamp et al., 1992; Kudva et al., 1996; Van der Wijst et al., 1997, Strelec and Lagoudas, 2002). This approach was used by Beauchamp et al. (1992) to create an adjustable camber control fin in which the leading and trailing edge were connected with a spring backbone and SMA wire, while Kudva et al. (1996) have embedded SMA tubes into control surfaces to twist a wing tip. Later Strelec and Lagoudas (2002) attached SMA wires to the inside of an airfoil to alter its shape. It is important to realize that when heating of the SMA wires ceases, the SMA wires may undergo martensite transformation. Such devices therefore require a continuous power input to maintain new shapes.

Significant research has sought to develop two-way shape memory actuators to overcome these problems (Saburi and Nenno, 1974; Schroeder and Wayman, 1977). The two-way shape memory effect can be created in some SMAs using thermomechanical training treatments. The internal stress thereby introduced in the microstructure then acts as the bias force (Otsuka and Wayman, 1998). Unfortunately reversing actuator designs based on the two-way shape memory effect has

\*Author to whom correspondence should be addressed.

E-mail: aarash@virginia.edu

Figures 1-3 and 7 appear in color online: <http://jim.sagepub.com>

met with limited success because of the low recovery strain on cooling ( $<2\%$ ) compared to that achieved by heating (6–8%) and the very low transformation forces generated upon cooling (Duerig, 1990). A recent example of a proposed application of this approach is the work of Lu et al. (2001) who analyzed a flexural actuating panel incorporating two-way SMA face sheets bonded to a truss core. Their actuator promised to achieve fully reversible actuation if the extension of the two-way SMA upon cooling could equal the contraction of the alloy upon heating.

Antagonistic (differential) methods have also been used to create reversible actuating joints in which contraction (upon heating) of one pre-stretched actuator results in the stretching of an opposing actuator, thus preparing it to be heated later in the cycle. Bergamasco et al. (1990) used this approach to design a robotic finger joint which used two active SMA springs in an antagonistic arrangement, while Van der Wijst et al. (1997) assembled two SMA wires at opposite edges of a rectangular hinged beam to rotate it. By connecting more beams together and using a feedback controller, they were able to change the curvature of the assembled structure. The authors have investigated fully reversible antagonistic shape morphing flexural beams (Elzey et al., 2002, 2003, 2005; Sofla et al. 2004). The antagonistic approach eliminates the need for additional bias force components, thereby reducing the structure's weight and complexity (Elzey et al., 2005) and increasing the work that can be done by the actuator against externally applied loads. These antagonistic actuating devices do not require continuous power to retain the new shapes after deactivation, and are therefore particularly well-suited for long-term applications in which the structure does not carry large loads, such as a space antenna or on/off switches. The beam in Figure 1(a) uses a pair of pre-stretched one-way SMA strips on either side of a corrugated core to create a simple sandwich structure (Elzey et al., 2002). The actuation strains associated with the one-way effect enabled tip deflections of up to 8% of the span length. The design was later improved by modifying the core topology and the shape memory pre-strain (Elzey et al., 2005). The improved beam achieved a cantilever tip displacement of 55% of the beam span. Subsequent developments have replaced the core with a structure that used freely rotating, revolute joints between the unit cells (Elzey et al., 2003). This significantly reduced the stored elastic energy in the core. Each of these devices consisted of a series of linearly repeating antagonistic flexural unit cells (AFC) (Sofla et al., 2004), shown in Figure 1. Experiments indicate that the tip deflections of these flexural structures are highly sensitive to the thermo-mechanical response of the SMA (Sofla et al., 2004).

Here the effect of the SMA pre-strain on the actuation strains for near equiatomic NiTi alloys is investigated

and the behavior to microstructural changes in the actuators during heating and cooling is related. An *in situ* experiment is introduced to directly measure the strain recovery and stresses in a pair of NiTi ribbons which are antagonistically connected. The experiments have been conducted on structures that used actuators that had been subjected to several different shape memory pre-strains. The deformations of these prototype beams compare favorably with a model of the system, indicating that it can be used for the design of more efficient, antagonistic SMA actuated structures.

## ANTAGONISTIC FLEXURAL ACTUATING CELL

A generalized AFC that enables reversible flexural morphing of a structure using one-way SMA linear actuating elements is shown in Figure 2. The unit cell consists of two rigid bodies of arbitrary shape attached at a freely rotating pivot point. The two bodies are attached to a pair of opposing linear actuators positioned on opposite sides of the pivot. Contraction

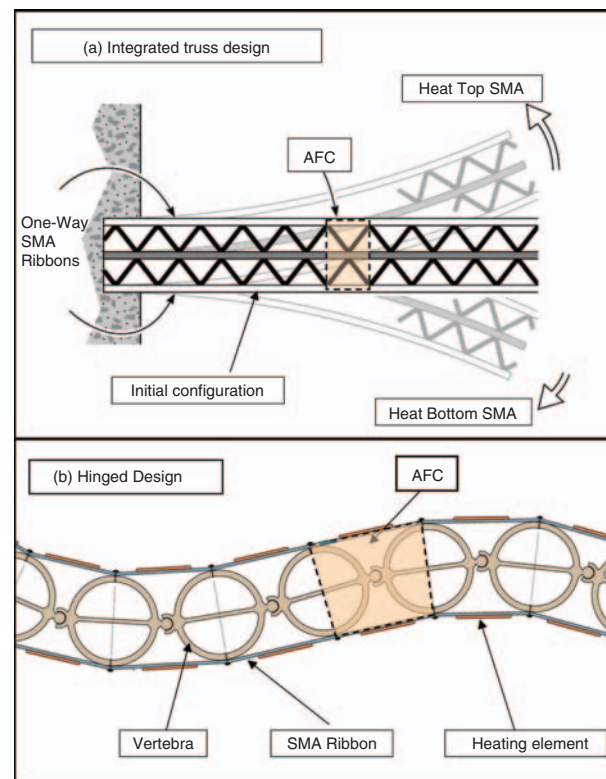


**Figure 1.** (a) A cantilever sandwich beam constructed from a triangular corrugated core and pre-strained shape memory alloy face sheets. Heating of one of the face sheets causes contraction of that face sheet, and consequent tensile elongation of the non-heated face sheet, and an overall flexural deformation of the beam (after Elzey et al., 2005) and (b) an alternative design in which the core facilitates bending between the adjacent unit cells via rotation joints (vertebra). This reduces the stored elastic energy in the core and permits higher authority actuation. (After Elzey et al. (2003)).

of either of the linear elements rotates the rigid bodies about the joint and stretches the opposite linear element. Subsequent heating of the newly stretched actuator results in a two-way structural response. The structure behaves antagonistically since neither actuator in the cell can be contracted without extending its opposing counterpart. The beams shown in Figure 1 were created by linking several of these AFCs.

The shape memory effect in NiTi alloys originates from the twinning/detwinning of the martensite phase of near equiatomic NiTi (Otsuka and Wayman, 1998). Cooling the austenite (B2) phase of NiTi below its martensite start temperature ( $M_s$ ) then initiates a transformation to the B19' martensitic structure (Otsuka and Wayman, 1998). An intermediate rhombohedral phase (R-phase) can also appear in some of the NiTi alloys during transformation from the B2 to the B19' structure (Otsuka and Wayman, 1998).

The transformation to martensite takes place in a self-accommodating manner to create a highly twinned martensite (TM), leaving the macroscopic dimensions of the ribbon only slightly changed (by the normal thermal contraction strain) (Otsuka and Wayman, 1998). However, the interfaces of the twinned B19' martensite variants are highly mobile (Otsuka, 1971; Saburi and Nenno, 1982), and an applied strain can be accommodated by the movement of twin boundaries (detwinning) which in turn enables the SMA ribbon to inelastically deform at quite low stress. Ultimately the B19' martensite variant which gives the largest transformation strain in the applied stress direction becomes preferred over other variants (Otsuka and Wayman, 1998). This structure is referred to as detwinned martensite (DM). The detwinning deformation differs from the plastic deformation involving dislocations because the detwinning deformation can be fully removed (the shape memory effect) when the SMA is heated above the austenite finish temperature ( $A_f$ ) to reform the original cubic B2 structure.

The NiTi alloy used in the AFC structure should therefore have a martensite finish temperature ( $M_f$ ) above ambient so that the natural cooling of the NiTi actuators fully transforms the A-phase to M-phase. It has also been observed (see the next section) that a NiTi alloy exhibiting the rhombohedral phase (R-phase), with  $M_f$  below ambient, can also be used in an AFC provided the R-phase transformation temperatures are above ambient.

A shape memory pre-strain can be imparted to the AFC shown in Figure 2 by mechanically stretching a ribbon (or wire) of NiTi at temperatures below its  $M_s$  temperature, prior to assembly of the unit cell. The stored pre-strain in the ribbon determines the achievable rotation of the cell, as well as the forces that can be induced in the structure. This in turn determines the maximum work that can be performed by the device.

The stored shape memory pre-strain in the top element (Figure 2) is denoted  $\varepsilon_1^s$ , while that of the bottom element is  $\varepsilon_2^s$ . The pre-strains can be arbitrary in the sense that one of the elements could be pre-strained, while the pre-strain in the opposing element could be set to zero. Contraction of linear actuator 1, rotates the cell to an angular position,  $\theta_1$  defined in Figure 2.

If the cell height ( $H$ ) is assumed unchanged during the cell rotation, a geometrical argument (Sofla et al., 2004) gives an expression for the angular rotation:

$$\theta_1 = 2 \tan^{-1} \left( \frac{L}{H} \right) - \cos^{-1} \left[ 1 - \frac{2(1 + \varepsilon_1 - \varepsilon_1^s)^2}{1 + (H/L)^2} \right] \quad (1)$$

where  $L$  is the actuator length in the initial configuration (prior to activation of the assembled cell), and  $\varepsilon_1$  is the remaining strain in actuated SMA element 1 (based upon the original actuator length prior to pre-straining). The remaining strain ( $\varepsilon_1$ ) and therefore the rotation of the unit cell, can be controlled through manipulation of the actuator's temperature. Here, the limiting deformation of the cell is considered (corresponding to complete transformation of the DT B19' structure to austenite within the actuated element).

There are four possible geometric configurations for an AFC, based on the two (DT B19'/B2) limiting states for each of the linear actuators. These deformations can be visualized using an equivalent linear arrangement of the SMA members in an antagonistic system, as shown in Figure 3. The pre-straining process is illustrated in Figure 3(a)–(e). An as-received SMA ribbon or wire (Figure 3(a)) is heated to remove previously stored (processing induced) strains (Figure 3(b)). Cooling the

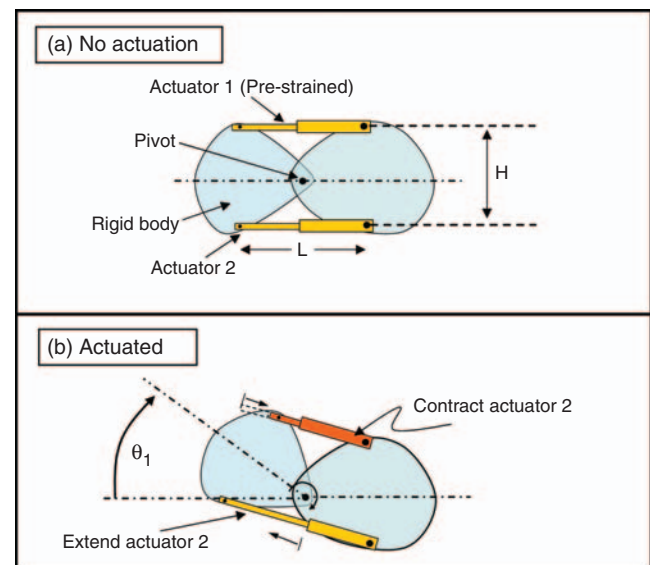


**Figure 2.** A generalized antagonistic flexural cell (AFC) consisting of a pair of arbitrarily shaped rigid bodies joined at a pivot point: (a) linear actuator elements are in the neutral position prior to actuation and (b) actuation (contraction) of the top element causes the bottom element to be extended and the cell to rotate.

actuator to ambient temperature is assumed to have no effect on the actuator's length (Figure 3(c)). The actuator is then strained (Figure 3(d)) and subsequently unloaded (Figure 3(e)). A shape memory strain ( $\epsilon_1^s$ ) is then stored in the ribbon as part of the TM transformed to DM during pre-straining. The pre-strained actuator is then attached to a same length non-prestrained actuator at one end with the remaining ends fixed. The connection between the two actuators is marked by a black dot in the figure for clarity.

After heating the top, pre-strained actuator above its  $A_s$  temperature, the B19'-phase begins to transform to austenite. The transformation of the DM then results in the contraction of the SMA ribbon, which antagonistically strains (extends) the opposite ribbon. As the temperature of Actuator 1 is increased, the joint between the two SMA members is displaced upwards (Figure 3(g)). However, the resulting antagonistic force prevents full transformation of the top ribbon to austenite ( $\epsilon_1$  does not reach zero) above the  $A_f$  temperature due to the stress-induced martensite (SIM) (Otsuka and Wayman, 1998). The strain remaining after accomplishment of all possible transformation upon heating is called the active equilibrium strain ( $\epsilon_1^a$ ) and is necessarily larger than zero. The displacement corresponding to this strain is

shown in Figure 3(g). This displacement is unknown and must be determined to deduce the actuator deformations defined by Equation (1).

The displacement shown in Figure 3(g) changes slightly if heating is terminated, since during cooling, the austenite phase of Actuator 1 transforms to the B19'-phase. Part of the new martensite is further detwinned due to the presence of antagonistic stresses. This results in the extension of the now-cooled Actuator 1, causing the joint to be displaced downwards slightly (Figure 3(h)). The new elongation of Actuator 1 simultaneously relaxes Actuator 2, which experiences an elastic unloading. Mechanical equilibrium is reached when detwinning in SMA Actuator 1 stops and further unloading of Actuator 2 ceases. The strain at this point is called the inactive equilibrium strain ( $\epsilon_1^i$ ), Figure 3(h). This new position needs no continuous heating to be retained and therefore represents a significant technological advantage for this type of SMA-based actuator design. States (g) and (h) in Figure 3 correspond to upward rotation of the rigid bodies in Figure 2 when the top actuator is heated and a slight downward relaxation occurs because of the deactivation of the top actuator.

Similar transformations occur when, the now-strained, Actuator 2 is heated creating configuration (i)

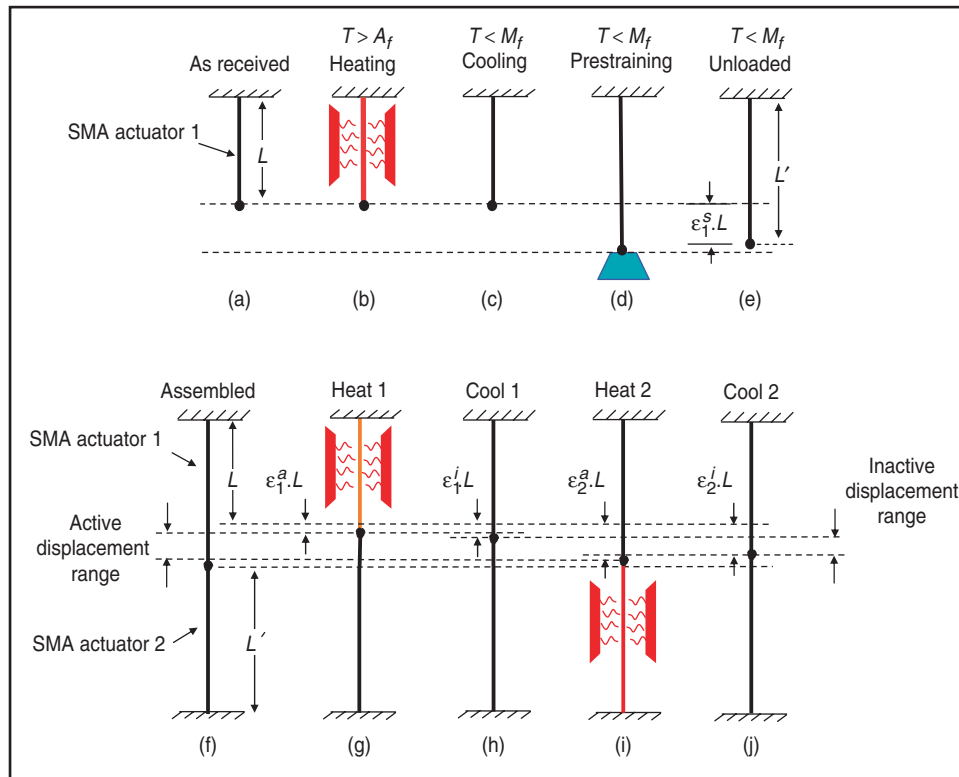


**Figure 3.** Sequence of states during pre-straining and the first thermomechanical cycle of a two-way linear antagonistic actuator analogous to AFC: (a) As received SMA ribbon or wire, (b) stored strains are removed upon heating, (c) cooling to room temperature (with no length change upon cooling), (d) the actuator is strained, (e) the actuator is unloaded, a permanent shape memory strain is stored, (f) the linear actuator is assembled to an antagonistic linear cell by connecting to a non pre-strained ribbon and fixing the free ends, (g) the pre-strained ribbon contracts when heated (though not all pre-strain is recovered due to SIM), (h) the heated actuator is cooled to room  $T$ , and relaxes slightly (i) the opposite ribbon is heated, straining the first one, (j) the opposite element is cooled and therefore relaxes slightly.

in Figure 3, and subsequently cooled (j). A total of four distinct configurations can therefore be attained during a complete cycle, corresponding to heating Actuator 1, cooling Actuator 1, heating Actuator 2, and cooling Actuator 2. In Figure 3, the ‘active displacement’ range is the displacement between the two active states (g) and (i), while the ‘inactive displacement’ range is the displacement between the two cooled states (h) and (j), which require no heating.

The thermomechanical process of pre-straining Actuator 1 as shown in Figure 3(a)–(e), assembly (f), and the first complete actuation cycle after the assembly (Figure 3(g)–(i)) are also schematically illustrated in Figure 4. The top left graph in Figure 4 shows the change of strain in Actuator 1 as the temperature of Actuator 1 is changed. The graphs on the right side of Figure 4 show the stress and temperature in Actuator 2 versus strain in Actuator 2. The strain in Actuator 2 is not shown in the next figures since it is simply related to the strain in Actuator 1. This can be seen by recognizing that the contractile displacement of Actuator 1 is the same as the extensional displacement of Actuator 2. If both actuators are assembled with the same initial length,  $L' = (L + \varepsilon_1^s \cdot L)$ , the magnitude of the engineering strain change in the actuators must be the same (i.e.,  $\varepsilon_1 - \varepsilon_1^s = -(\varepsilon_2 - \varepsilon_2^s)$ ). This then gives a relationship

for the strain in Actuator 2 ( $\varepsilon_2$ ) in terms of the stored strain in both actuators ( $\varepsilon_1^s$  and  $\varepsilon_2^s$ ) and the strain in Actuator 1,  $\varepsilon_1$ :

$$\varepsilon_1 = \varepsilon_1^s + \varepsilon_2^s - \varepsilon_2. \quad (2)$$

The lower graphs in Figure 4 schematically show the change of stress in the actuators during pre-straining and the first actuation cycle. In the absence of an applied load, both actuators experience equal stress. The relative amounts of shape memory pre-strain and active and inactive equilibrium strains can be compared at the bottom of Figure 4.

## EXPERIMENTAL ASSESSMENT

A model incorporating the thermomechanical behavior of the SMA actuator described here could be used with the equations of mechanical equilibrium to determine the deformations and forces of the AFC (Sofla et al., 2004). However, such an approach is currently limited by the need for a large number of empirically determined material coefficients and by simplified transformation kinetics, which do not explicitly address hysteresis (Saburi and Nenno, 1982; Duerig et al., 1990). Instead, antagonistic experiments have

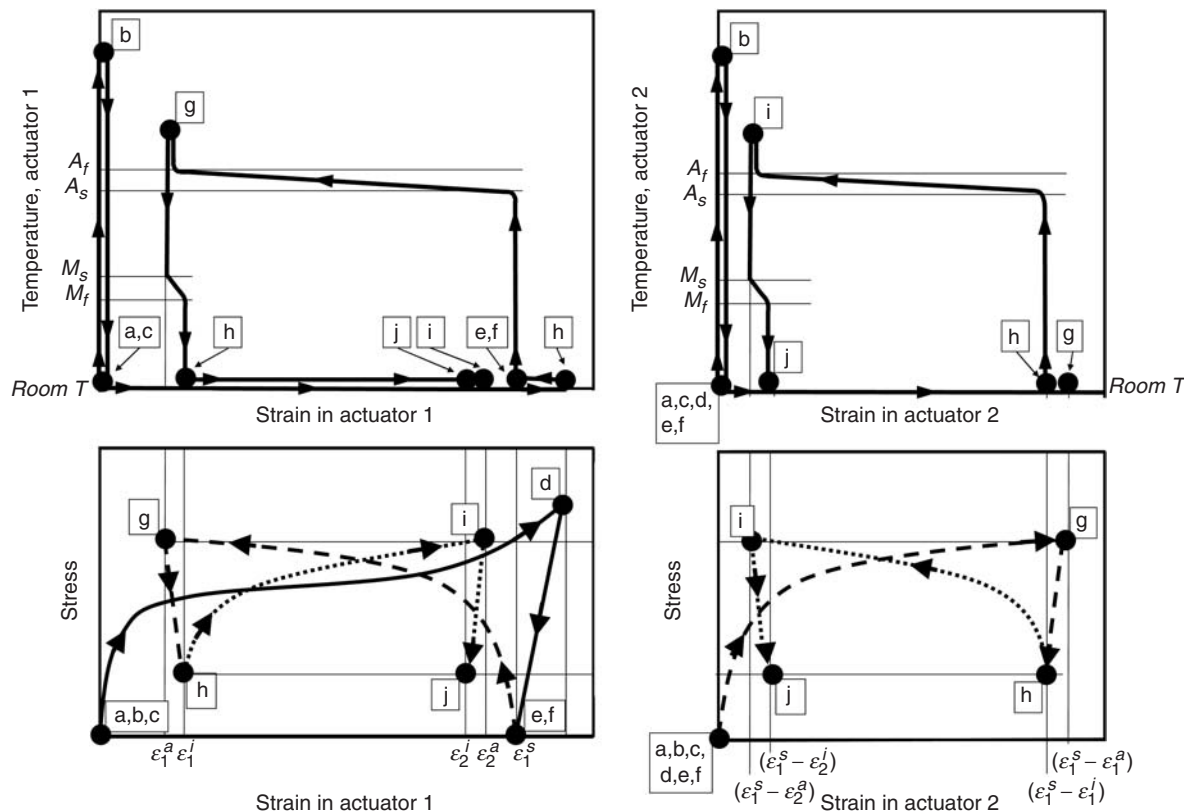


**Figure 4.** Left – The temperature and stress versus strain in Actuator 1 of an as-received SMA ribbon during pre-straining and assembly of an antagonistic cell (a–e). The temperature–stress–strain during the first actuation cycle of the cell (f–j) is also shown. a–j states are the same as those identified in Figure 3. Right – The temperature and stress versus strain in Actuator 2.

been conducted to directly measure the deformations and forces created by a representative SMA ribbon in an antagonistic unit cell. The transformation temperatures and stress–strain response of near equiatomic NiTi ribbons were first determined using differential scanning calorimetry (DSC) experiment and tensile testing.

### DSC Results

Near equiatomic, Ni-50.6at%Ti ribbons supplied by Nitinol Devices and Components (Fremont, CA) were used in this study. A differential scanning calorimeter (DSC) was used to determine the unstressed transformation temperatures of the alloy (Otsuka and Wayman, 1998). Figure 5 shows a typical DSC test result conducted for a 33 mg ribbon sample. Upon cooling (see top, exothermic curve), two separate peaks appear, consistent with the A-phase changes to a rhombohedral R-phase, followed by a transformation to the M-phase (Nam et al., 2002; Wang et al., 2005). The martensite start and finish transformation temperatures ( $M_s$  and  $M_f$ ) for the data shown in Figure 5 were found to be 23 and  $-3^\circ\text{C}$ . The austenite start and finish temperatures ( $A_s$  and  $A_f$ ) were 56 and  $69^\circ\text{C}$  while the R-phase start and finish temperatures ( $R_s$ ,  $R_f$ ) were 51 and  $43^\circ\text{C}$  (obtained using the tangent line method). As  $M_s$  for this sample is below the ambient temperature ( $25^\circ\text{C}$ ), the stress-free ribbons were in the R-phase after cooling to room temperature. The intermediate R-phase has a trigonal structure (Otsuka and Wayman, 1998) and undergoes a transformation to SIM, DM

(B19' structure) under the action of external forces (Miyazaki and Otsuka, 1986). If the cooling takes place at an applied stress similar to that created by the antagonistic interaction forces, then the R-phase could change to martensite above the  $M_s$  temperature (Sittner et al., 2004).

Fully reversible actuating devices previously fabricated using the same NiTi alloy have confirmed that NiTi alloy compositions possessing intermediate R-phase, with R-phase transformation temperatures above room temperature, can be used as linear actuators in antagonistic shape morphing structures (Elzey et al., 2002, 2003, 2005; Sofla et al. 2004).

### Tensile Test Results

The stress–strain relationship of the SMA ribbons depends on the phases present, which consequently affects the responses of the AFC actuator. Figure 6 shows the stress–strain curves of six initially identical samples heated to  $180^\circ\text{C}$ . One was subsequently cooled to room temperature (which is between the alloy's  $M_s$  and  $R_f$ ) while another was cooled to  $-80^\circ\text{C}$  which is below the sample's  $M_f$  temperature as determined by the DSC experiment (Figure 5). The other four samples were cooled to 2, 7, 12, and  $17^\circ\text{C}$  (within the  $M_s - M_f$  range of this NiTi alloy). Although all samples were tested at room temperature, Figure 6 indicates that the stress required for changing TM to DM (in the predominantly M-phase samples) is larger than the stress needed to transform the predominantly

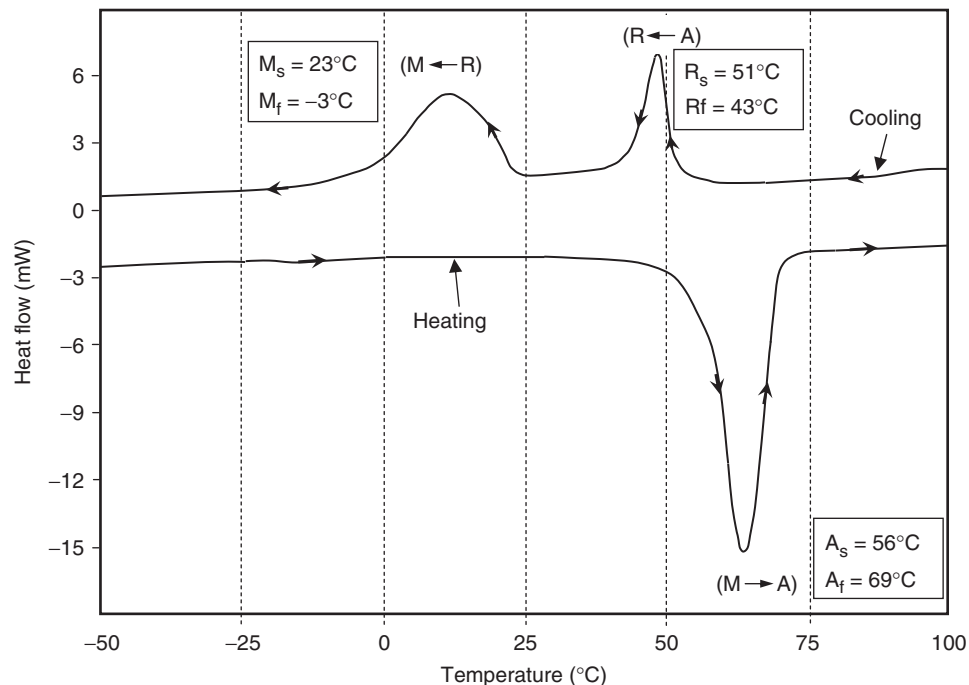
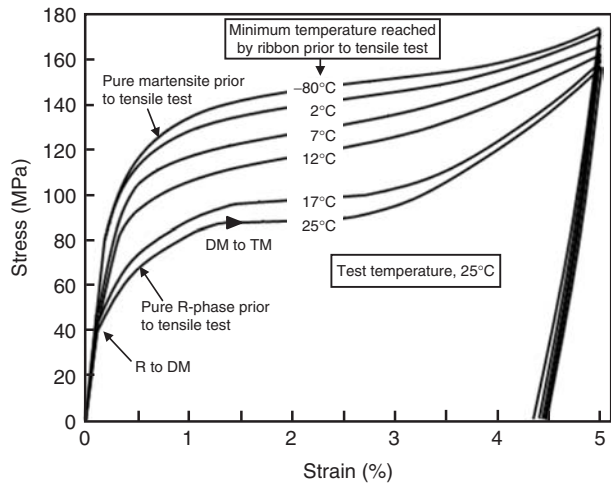


Figure 5. Differential scanning calorimetry (DSC) reveals the transformation temperatures of a Ni-50.6at%Ti ribbon.

R-phase sample to DM. This observation agrees well with experimental results reported by Lach et al. (2002) where they compared the stress–strain relationships of ‘recovered’ ribbons (those cooled to between  $M_s$  and  $R_f$ ) with ‘recovered frozen’ ribbons (cooled below  $M_f$ ). It is noted that the selection of a NiTi alloy composition with a  $M_f$  below ambient results in lower antagonistic forces



**Figure 6.** Stress–strain curves for six ribbons cooled to different temperatures prior to tensile testing. The final temperatures reached on cooling range from well below the  $M_f$  to just above  $M_s$  temperatures. Samples with a large R-phase content can be detwinned at lower stress than fully martensitic samples.

than one with  $M_f$  near or above ambient. This favorably impacts the ability of AFC-based devices to achieve large deformations.

### In situ Antagonistic Experiment

Antagonistic experiments were conducted to directly measure the shape recovery strain and the forces in a representative linear antagonistic actuator, with the test setup schematically illustrated in Figure 7. Two identical, Ni-50.6at%Ti ribbons, each 0.25 mm thick and 7 mm wide were first heated to 180°C, which is well above the alloy’s  $A_f$  temperature (69°C), for 30 s. This removed any stored shape memory strain developed during ribbon fabrication. The ribbons were then cooled to room temperature. One ribbon (Ribbon 1 in Figure 7) was then pre-strained 4.5% and mounted in series with a similar, but shape memory strain-free, ribbon (Ribbon 2) in the test fixture. The ribbons are connected by a mechanical fastener that also served to insulate the two ribbons, thermally and electrically. The two free ends of the test structure were then fixed in the grips of a tensile test machine and a load cell was used to monitor the force generated in the ribbons during an antagonistic test. The gage length of the two ribbons prior to the start of the experiment was 80 mm ( $L'$  in Figure 3(e) and (f)). The subsequent strain in Ribbon 1 was then measured using a laser extensometer as it was thermally cycled.

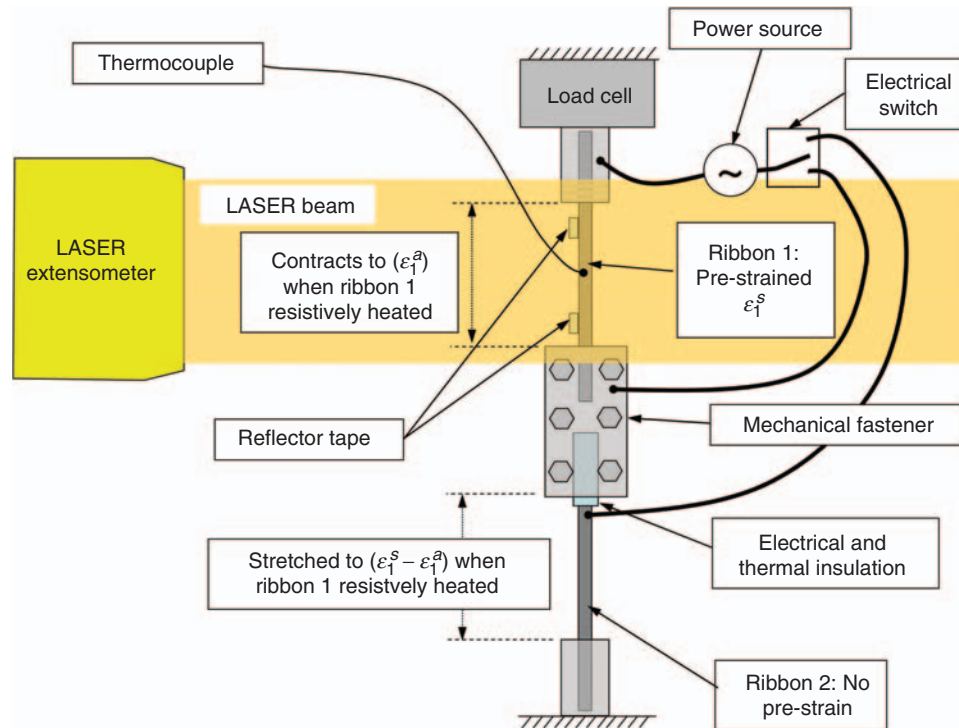


**Figure 7.** In situ antagonistic experimental setup used to find the recovery strain and stresses during actuation/de-activation of either actuator in a linear antagonistic cell.

Thermocouples attached to the SMA actuators were used to monitor their respective temperatures.

The antagonistic experiment was initiated by heating Ribbon 1 to 110°C, a temperature above the alloy's  $A_f$  temperature (69°C). This resulted in a contraction to strain  $\varepsilon_1^a$  (Position (g) in Figure 3). The heating rate was about 1°C/s and was controlled by manual adjustment of the input power. Additional heating was avoided since this could result in thermal expansion of the ribbon, thereby increasing the active equilibrium strain (a larger  $\varepsilon_1^a$  means a smaller displacement of Actuator 1) and reducing the antagonistic force. The heating was then terminated and the ribbon was allowed to cool naturally to room temperature (Position (h) in Figure 3), relaxing slightly as it did so.

In the next step, Ribbon 2 was heated (Position (i) in Figure 3), stretching Ribbon 1. It was then cooled to room temperature (Position (j) in Figure 3). The force in the ribbons was recorded by the load cell, and was converted to stress and is plotted as a function of strain for Ribbon 1 in Figure 8. The figure shows the stress-strain relationship during the first antagonistic cycle (Stages (f), (g)) for an experiment using a 4.5% initial shape memory pre-strain. The prior stress-strain response during the pre-straining process (Stages (a)–(e)) is also shown for comparison. The points of interest in Figure 8 are marked with letters consistent with the labeling used in Figures 3 and 4. The characteristic strains for the 4.5% pre-strained ribbon case were measured using the data in Figure 8 and used to predict the deformations of an antagonistic flexural cell.

An antagonistic SMA actuated device works reversibly provided the stress created during the austenite transformation of the pre-strained linear actuator exceeds the stress to deform (detwin) its low

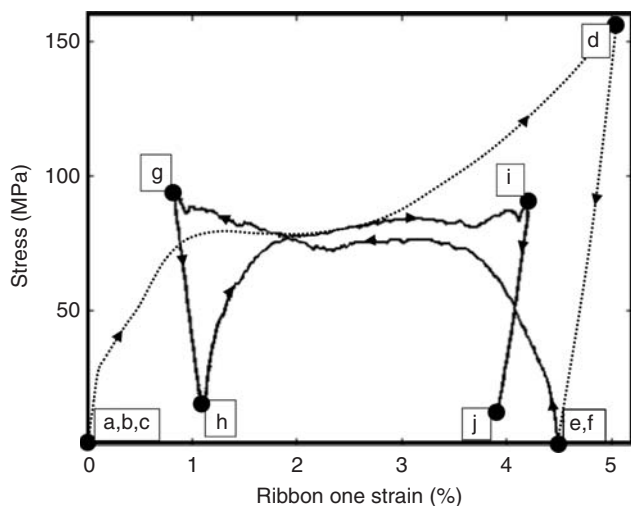


**Figure 8.** Stress in the SMA Ribbons 1 and 2 versus strain of Ribbon 1 during successive actuation and deactivation of either ribbon in the antagonistic unit cell. The pre-strain in Ribbon 1 before the assembly was 4.5%. The stress-strain relationship of the ribbon during pre-straining is superimposed on the graph as a dotted line.

temperature martensitic counterpart. Figure 9 shows the stress created in a pre-strained NiTi ribbon during heating. The ribbon is fixed at both ends such that the ribbon's strain is constant during heating. The approximate maximum stresses of 450, 550, and 650 MPa have been observed for pre-strains 2.5, 3.5, and 4.5%. Comparing these stresses with the stress needed to plastically deform (detwin) the ribbon at low temperature (Figure 6) reveals that the stress created during heating significantly exceeds that needed to deform the low-temperature phase (<100 MPa). As shown in Figure 8, the stress induced in the actuators upon heating one of them is less than the maximum stress shown in Figure 9 because one of the actuators is always in the low temperature phase. The antagonistic interaction requires both actuators to experience identical axial stress therefore the stress created by heating one of them must be equal to the stress required to deform the lower strength, low temperature actuator (about 100 MPa), Figure 8.

To investigate the effect of shape memory pre-strain on the deformation range of the antagonistic actuating structure, the experiment was repeated with shape memory pre-strains of 2.5, 4, 5, 6, and 7%. Only the recorded inactive strains versus pre-strain are shown in Figure 10, owing to the importance of inactive deformations for long-term applications. Figure 10 shows that increasing the amount of pre-strain results in a larger attainable strain (deformation) range. Therefore, expectedly, high authority actuated structures are achieved by increasing the imparted SMA pre-strain to the structure. The graph can also be used to determine the required pre-strain in the preliminary design of actuated structures having specified deformations.

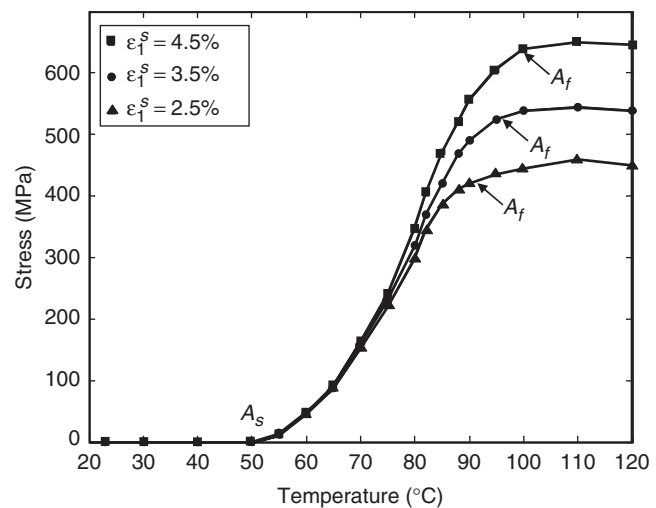


**Figure 9.** The influence of pre-strain on the actuation strength for NiTi ribbons fixed at both ends while heated above the austenite finish temperature.

In the DSC experiment, no external forces act on the sample. In general, the transformation temperatures of NiTi alloys increase with stress in an approximately linear fashion (Duerig, 1990). This can be seen in Figure 9. The austenite start temperature is the same for all three samples (because they are initially stress free), while the austenite finish temperature increases for the ribbons with increasing pre-strain. Therefore, the effect of the stress on the transformation temperatures needs to be considered in the heat transfer analysis of an actuator.

## DISCUSSION

The representative stress–strain curve resulting from the antagonistic test (i.e., the plot for a setup with a 4.5% pre-strained ribbon, Figure 8) contains information which can be used to determine the recovery strains and stresses of the actuating cell. In addition, the recovery strains can be used to determine the limiting rotation angles of an AFC (Figure 2) incorporating 4.5% pre-strain. The active equilibrium strain for actuation of Ribbon 1 ( $\varepsilon_1^a$ ), which defines the cell shape upon heating Ribbon 1 above  $A_f$ , is marked by ‘g’ in Figure 8. This strain corresponds to 0.84%, meaning the 4.5% shape memory pre-strain in Ribbon 1 is not fully recovered upon heating above  $A_f$  (the antagonistic interaction force in the ribbons creates some detwinned SIM). Similarly, the active equilibrium strain upon heating Ribbon 2 ( $\varepsilon_2^a$ ) is determined to be 4.19% (labeled as ‘i’ in Figure 8).

The angular rotations of an actuated AFC (Figure 2) can be determined using Equation (1) by substituting

$\varepsilon_1^a = 0.84\%$  and choosing the height to length ratio of the cell (chosen to be 0.778 in this case of a sample AFC).

$$\theta_1^a = 2 \tan^{-1} \left( \frac{1}{0.778} \right) - \cos^{-1} \left[ 1 - \frac{2(1 + 0.0084 - 0.045)^2}{1 + (0.778)^2} \right] = 5.24^\circ.$$

Thus the cell in Figure 2 is rotated  $5.24^\circ$  upward upon actuating Ribbon 1. Similarly, the configuration of the cell after heating Ribbon 2 is,

$$\theta_2^a = 2 \tan^{-1}(1 - 0.778) - \cos^{-1} \left[ 1 - \frac{2(1 + 0.0419 - 0.045)^2}{1 + (0.778)^2} \right] = 0.45^\circ,$$

meaning the cell is partially returned toward its original flat shape. However, the flat shape is not fully recovered because of the SIM in Ribbon 2. The active deformation range for a cell with one of its ribbons pre-strained to 4.5% is therefore determined to be  $4.79^\circ$  ( $5.24^\circ - 0.45^\circ = 4.79^\circ$ ). This means the actuated unit cell can morph up to  $4.79^\circ$  during its actuation cycle. This deformation range for the actuator persists, assuming no plastic deformation is introduced to the structure in subsequent cycles. Although not focus of this study, the shape degradation of the cell can be investigated by repeating the thermomechanical cycle during antagonistic testing.

The inactive equilibrium strain after cooling Ribbon 1 (Point h),  $\varepsilon_1^i$ , is found to be 1.09% and upon cooling Ribbon 2 (Point j),  $\varepsilon_2^i$ , 3.85%. These deformations are maintained at room temperature until the cell is activated again. The corresponding rotation angles for the cell are determined to be  $4.49^\circ$  and  $0.95^\circ$ . The inactive deformation range is found to be  $4.49^\circ - 0.95^\circ = 3.54^\circ$  in a similar manner. Therefore the final low temperature deformations are substantially different (i.e., by  $3.54^\circ$ ). These low temperature configurations need no external energy to be retained.

The four characteristic configurations of the cell in a cycle of actuation/deactivation of either ribbons are then summarized as:  $5.24^\circ$  upward rotation upon heating Ribbon 1 (configuration g), downward relaxation of the cell to angular position  $4.49^\circ$  upon cooling Ribbon 1 to room temperature (h), then more downward rotation of the cell to angle  $0.45^\circ$  upon heating Ribbon 2 (i), and finally upward relaxation to the angle  $0.95^\circ$  after cooling Ribbon 2 (j).

The active equilibrium stress is found to be 94 MPa upon heating Ribbon 1 (stress at configuration g) and 92 MPa upon heating Ribbon 2 (i). The inactive equilibrium stress is found to be 15 MPa upon cooling Ribbon 1 (h) and 13 MPa upon cooling Ribbon 2 (j).

The measured inactive strains for different pre-strains (Figure 10) are substituted into Equation (1) to estimate

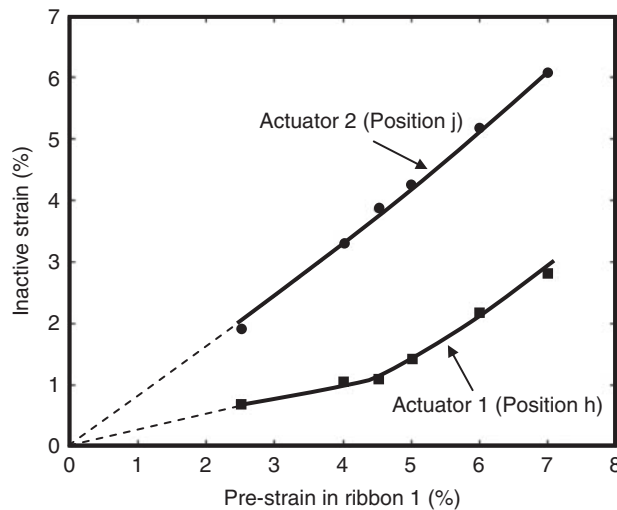


**Figure 10.** Inactive strain versus pre-strain. For each pre-strain, the inactive range can be found by subtracting the two inactive equilibrium strains. Configurations, h and j are as defined in Figure 8.

the inactive rotation angles of a sample AFC ( $H/L=0.778$ ). The top curve in Figure 11 shows the predicted rotation angle if the top actuator (Figure 2) is heated and cooled while the bottom curve is the predicted rotation angle after heating and cooling of the bottom actuator. AFC prototypes similar to Figure 1(b) were fabricated to verify the predicted values by connecting two steel tubes connected via a low friction revolute joint. Two SMA ribbons (the same ribbons used in the *in situ* antagonistic test) were fixed to the sides of the joint by means of mechanical fasteners. Electrically insulated resistive wires were helically wrapped around the ribbons for heating. Three samples with 2.5, 4.5, and 7.0% pre-strain were then fabricated and tested. The rotation angles were measured and plotted in Figure 11 for comparison. The measured deformations of the AFC samples are in good agreement with predicted values from the *in situ* antagonistic experiment (within 5% absolute). The measured rotation angle after heating and cooling the top ribbon (hollow square in Figure 11) is slightly smaller than the corresponding predicted value (black square) in all the three samples. This may be due to friction at the joint and some slack in the ribbons after assembly (prior to testing). Similarly, it can be seen that the rotation angle after activating the bottom ribbon (hollow circle in Figure 11) is somewhat larger than the predicted angle (black circle).

## CONCLUSIONS

Antagonistic flexural cells (AFC) can be used to create two-way SMA flexural actuators using a one-way

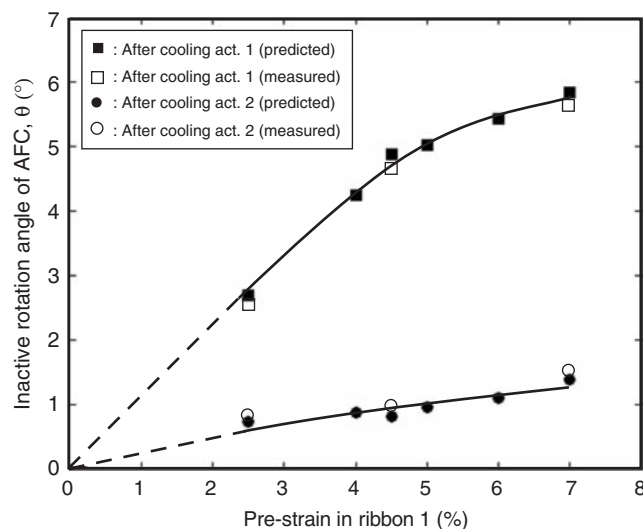


**Figure 11.** The inactive rotation angle of an AFC after heating and cooling the two actuators. The measured values lie within the predicted range.

shape memory effect. The cell provides four distinct positions for each segment of the actuator upon heating and cooling of either of the linear antagonistic actuators. In contrast to current bias force designs, two of the positions provided by the AFC require no external energy to be maintained, making the AFC suitable for devices requiring two different end shapes to be fixed for long periods. *In situ* antagonistic experiments were used to directly determine deformations (strains) and forces (stresses) in the antagonistic actuators. A sample experiment for a 4.5% pre-strained actuated unit cell resulted in a  $4.31^\circ$  inactive rotation range, implying that a beam made up of 84 such linked AFCs could switch between a flat shape and a full circle, while remaining in these configurations without the use of external power. Results from antagonistic experiments are in good agreement with the behavior observed for prototypes evaluated in previous studies. The AFC design is scalable (by means of assembly of the cells in 2D and 3D configurations) and is therefore applicable to a wide range of technologies from micro actuators and MEMS to aerospace and shape morphing structures and deployable structures.

## ACKNOWLEDGMENTS

The authors are grateful to Anthony Evans for useful discussions of this work. The research was supported in part by the Defense Advanced Research Projects Agency (Leo Christodoulou, program manager) and the Office of Naval Research (Steve Fishman, program manager) under grant number N00014-02-1-0614.

## REFERENCES

- Baz, A., Chen, T. and Ro, J. 2000. "Shape Control of NITINOL-reinforced Composite Beams," *Composites: Part B*, 31:631–642.
- Beauchamp, C.H., Nadolink, R.H., Dickinson, S.C. and Dean, L.M. 1992. "Shape Memory Alloy Adjustable Camber (SMAAC) Control Surfaces," In: *Proceedings of the 1<sup>st</sup> European Conference on Smart Structures and Materials*, pp. 189–192.
- Bergamasco, M., Dario, P. and Salsedo, F. 1990. "Shape Memory Alloy Microactuators," *Sensors and Actuators*, A21–A23:253–257.
- Crawly, E. 1994. "Intelligent Structures for Aerospace: A Technology Overview and Assessment," *AIAA Journal*, 32(8):1689–1699.
- Duerig, T.W., Melton, K.N., Stöckel, D. and Wayman, 1990. *Engineering Aspects of Shape Memory Alloys*, Butterworth-Heinemann Ltd, UK.
- Elzey, D.M., Sofla, A.Y.N. and Wadley, H.N.G. 2002. "Shape Memory-based Structural Actuator Panel," In: *Proceedings of the SPIE – The International Society for Optical Engineering*, Vol. 4698, pp. 192–200.
- Elzey, D.M., Sofla, A.Y.N. and Wadley, H.N.G. 2003. "A Bio-inspired, High Authority Actuator for Shape Morphing Structures," In: Lagoudas, D. (ed.), *Proceedings of SPIE*:

- Smart Structures and Materials: Active Materials Behavior and Mechanics*, Vol. 5053, pp. 92–100.
- Elzey, D.M., Sofla, A.Y.N. and Wadley, H.N.G. 2005. “A Shape Memory-based Multifunctional Structural Actuator Panel,” *International Journal of Solids and Structures*, 42:1943–1955.
- Giurgiutu, V. 2000. “Review of Smart-materials Actuation Solutions for Aeroelastic and Vibration Control,” *Journal of Intelligent Material Systems and Structures*, 11(7):525–544.
- Grag, D.P., Zikry, M.A. and Anderson, G.L. 2001. “Current and Potential Future Research Activities in Adaptive Structures: An ARO Prospective,” *Smart Materials and Structures*, 10(4):610–623.
- Kudva, J.N., Lockyer, A.J. and Appa, K. 1996. “Adaptive Aircraft Wing,” *AGARD Lecture Series 205, Smart Structures and Materials: Implications for Military Aircraft of New Generation*, Advisory Group for Aerospace Research and Development, Canada.
- Lach, C.L., Turner, T.L., Taminger, K.M. and Shenoy, R.N. 2002. “Effects of Thermomechanical History on Tensile Behavior of Nitinol Ribbon,” In: *Proceeding of SPIE – The International Society for Optical Engineering*, Vol. 4699, pp. 323–334, San Diego, CA.
- Lu, T.J., Hutchinson, J.W. and Evans, A.G. 2001. “Optimal Design of a Flexural Actuator,” *Journal of Mech. Phys. Solids*, 49(9):2071–2093.
- Miyazaki, S. and Otsuka, K. 1986. “Deformation and Transition Behavior Associated with the R-phase in Ti-Ni Alloys,” *Metallurgical Transactions*, 17A:53–63.
- Nam, T.H., Kim, J.H., Choi, M.S., Kim, Y.W., Im, H.J., Ahn, J.S. and Mitani, T. 2002. “R-phase Transformation in Equiatomic TiNi Alloy Ribbons Fabricated by Rapid Solidification,” *Journal of Materials Science Letters*, 21:685–688.
- Otsuka, K. 1971. “Origin of Memory Effect in Cu-Al-Ni Alloy,” *Japanese Journal of Applied Physics*, 10(5):571–579.
- Otsuka, K. and Wayman, C.M. 1998. *Shape Memory Materials*, Cambridge University Press, New York.
- Pelrine, R., Eckerle, J. and Chiba, S. 1992. “Review of Artificial Muscle Approaches,” In: *Proceeding of Third International Symposium on Micro Machine and Human Science*, Nagoya, Japan.
- Pfaeffle, H.J., Lagoudas, D.C., Tadjbakhsh, I.G. and Craig, K.C. 1993. “Design of Flexible Rods with Embedded SMA Actuators,” In: *Proceedings of SPIE*, Vol. 1917, pp. 762–773.
- Saburi, T. and Nenno, S. 1974. “Reversible Shape Memory in Cu-Zn-Ga,” *Scripta Metallurgica*, 8:1363–1368.
- Saburi, T. and Nenno, S. 1982. “Shape Memory Effect and Related Phenomena,” In: *Proceedings of International Conference On Solid-Solid Phase Transformations*, pp. 1455–1479, AIME, NY.
- Schroeder, T.A. and Wayman, C.M. 1977. “The Two-way Shape Memory Effect and Other “training” Phenomena in Cu–Zn Single Crystals,” *Scripta Metallurgica*, 11(3):225–230.
- Sittner, P., Lugovyy, D., Neov, D., Landa, M., Lukas, P. and Novak, V. 2004. “On the R-phase Transformation Related Phenomena in NiTi Polycrystals Subjected to Thermomechanical Loads,” *J. Phys. IV France*, 115:269–278.
- Sofla, A.Y.N., Elzey, D.M. and Wadley, H.N.G. 2004. “An Antagonistic Flexural Unit Cell for Design of Shape Morphing Structures,” In: *Proceedings of the ASME Aerospace Division: Adaptive Materials and Systems*, Aerospace Materials and Structures, pp. 261–269, Anaheim, CA.
- Strelec, J.K. and Lagoudas, D.C. 2002. “Fabrication and Testing of a Shape Memory Alloy Actuated Reconfigurable Wing,” In: *Proceedings of SPIE – The International Society for Optical Engineering*, Vol. 4701, pp. 267–280.
- Takagi, T. 1999. “Present State and Future of Intelligent Materials and Systems in Japan,” *Journal of Intelligent Material Systems and Structures*, 10(7):575–581.
- Tobushi, H., Hayashi, S. and Kojima, S. 1992. “Mechanical Properties of Shape Memory Polymer of Polyurethane Series,” *JSME International Journal, Series I (Solid Mechanics, Strength of Materials)*, 35(3):296–302.
- Uchino, K. 1997. *Piezoelectric Actuators and Ultrasonic Motors*, Kluwer Academic Publishers, Boston.
- Van der Wijst, M.W.M., Zuidervaart, J., Peijs, T. and Schreurs, P.J.G. 1997. “Active Shape Control of Shape Memory Alloy Composite Structures,” In: *Proceeding of ICCM-11*, pp. 561–570, Gold Coast, Australia.
- Wada, B.K. 1990. “Adaptive Structures – An Overview,” *Journal of Spacecraft and Rockets*, 27(3):330–337.
- Wang, Z.G., Zu, X.T. and Fu, Y.Q. 2005. “Study of Incomplete Transformations of Near Equiatomic TiNi Shape Memory Alloys by DSC Method,” *Materials Science & Engineering A (Structural Materials: Properties, Microstructure and Processing)*, 390(1–2):400–403.
- White, S.R. and Berman, J.B. 1998. “Thermomechanical Response of SMA Composite Beams with Embedded Nitinol Wires in an Epoxy Matrix,” *Journal of Intelligent Material Systems and Structures*, 9(5):391–400.

